Optics Letters

Laser power stabilization via radiation pressure

Marina Trad Nery,[1,*] Jasper R. Venneberg,[1] Nancy Aggarwal,[2] Garrett D. Cole,[3] Thomas Corbitt,[4] Jonathan Cripe,[4] Robert Lanza,[2] and Benno Willke[1]

[1]Max Planck Institute for Gravitational Physics (Albert Einstein Institute) and Institut für Gravitationsphysik, Leibniz Universität Hannover, Hannover, Germany
[2]LIGO Lab, MIT Kavli Institute, Department of Physics, MIT, Cambridge, Massachusetts 02139, USA
[3]Thorlabs Crystalline Solutions, Santa Barbara, California 93101, USA
[4]Louisiana State University, Department of Physics, Baton Rouge, Louisiana 70803, USA
*Corresponding author: marina.trad@aei.mpg.de

Received 17 February 2021; revised 17 March 2021; accepted 17 March 2021; posted 18 March 2021 (Doc. ID 422614); published 14 April 2021

This Letter reports the experimental realization of a novel, to the best of our knowledge, active power stabilization scheme in which laser power fluctuations are sensed via the radiation pressure driven motion they induce on a movable mirror. The mirror position and its fluctuations were determined by means of a weak auxiliary laser beam and a Michelson interferometer, which formed the in-loop sensor of the power stabilization feedback control system. This sensing technique exploits a nondemolition measurement, which can result in higher sensitivity for power fluctuations than direct, and hence destructive, detection. Here we used this new scheme in a proof-of-concept experiment to demonstrate power stabilization in the frequency range from 1 Hz to 10 kHz, limited at low frequencies by the thermal noise of the movable mirror at room temperature.

https://doi.org/10.1364/OL.422614

Laser power stabilization is essential for many modern experiments, since power noise is often a hindrance to their sensitivity [1–3]. The most demanding requirements on laser power noise at low frequencies were set by interferometric gravitational wave detectors, such as aLIGO detectors, where a relative power noise (RPN) of 2×10^{-9} $\mathrm{Hz}^{-1/2}$ is needed at 10 Hz [4]. Typically, to achieve high power stability, an active stabilization scheme comprising an in-loop sensor and a negative feedback control loop is implemented. The most common active scheme is the traditional scheme, where a small fraction of the laser power is picked off and sensed directly by a photodetector (PD). This scheme is fundamentally limited by shot noise of the detected light, which acts as sensing noise in the feedback loop and sets a limit to the minimum RPN that can be achieved in the out-of-loop (OOL) beam. Hence, the sensitivity of this scheme is given by the detected power P, and it scales proportionally to $P^{1/2}$. However, the amount of detected power required to achieve an RPN on the order of 10^{-9} $\mathrm{Hz}^{-1/2}$ is so large that it exceeds the working threshold of high efficiency and low noise PDs. Alternatives were adopted to circumvent this limitation such as implementing an array of photodiodes [5], reducing the detected shot noise by injection of squeezed vacuum [6], and sensing power fluctuations in reflection of an optical cavity [7]. Schemes exploiting nondemolition techniques were also investigated for power stabilization [8,9].

In this Letter, a new scheme for power stabilization is experimentally investigated. Here, the power fluctuations of a strong laser beam to be stabilized, called the transfer beam, are transferred to the motion of a movable mirror. The position of the mirror and its fluctuations are determined by a Michelson interferometer (MI) employing a weak auxiliary beam, called the sensing beam. The interferometer containing the movable mirror represents the in-loop sensor of this stabilization scheme, which feeds back to a power actuator placed in the transfer beam path. This sensing technique exploits a nondemolition measurement [8], since the power fluctuations of the transfer beam are inferred by measuring the fluctuations in the phase observable of the auxiliary beam. This process results in higher signals representing transfer beam power fluctuations than what would be achieved by direct detection as in the traditional scheme [10]. The fundamental limit of this scheme, set by the quantum noise in the interferometer and the thermal noise of the movable mirror, was analyzed in [10]. The results showed that this scheme has the potential to achieve an RPN below 10^{-9} $\mathrm{Hz}^{-1/2}$. In addition to that, a power stabilization below the shot noise of the transfer beam should be possible, i.e., generation of a strong bright squeezed OOL beam. Another advantage is that the full transfer beam power is preserved and available for use. Hence, this new scheme could be implemented not only in future generations of gravitational wave detectors, but also in other high precision and optomechanical experiments. With all these foreseen advantages at hand, a proof-of-principle experiment was realized, and its results and limitations are reported herein.

The schematic of the experimental setup is shown in Fig. 1. A continuous-wave and single-frequency solid-state Nd:YAG nonplanar ring oscillator (NPRO) was used as a laser source. Approximately 90% of its output light was reflected to the transfer beam path, while the remaining light was transmitted to the sensing beam path. The transfer beam was then sent to an acousto-optic modulator (AOM), which was the power actuator chosen for this setup. To prevent the scattered light

Corrected 14 April 2021

of the transfer beam from coupling to the interferometer displacement readout, the first-order beam transmitted by the AOM (frequency shifted by 80 MHz) was the beam used in this experiment. An attenuation stage formed by a polarizing beam splitter (PBS) and a half-wave plate was placed after the AOM to adjust the power on the movable mirror. The transfer and sensing beams were guided via two single-mode and polarization-maintaining optical fibers into a vacuum chamber, where a breadboard containing the MI was placed. The interferometer comprised a 50:50 cubic beam splitter, a rigidly supported high reflective mirror, and a micro-oscillator mirror (movable mirror). The rigidly supported mirror was attached to a piezoelectric transducer (PZT), which was used as a position actuator to stabilize the interferometer at the mid-fringe operation point with a unity gain frequency (UGF) of 300 Hz. The mid-fringe operation point was chosen as it provides a linear relation of the interferometer's output power and the displacement of the micro-oscillator mirror. The output beam of the interferometer was then detected by a PD (MI PD), whose output voltage served as the error signal for the interferometer mid-fringe lock and also for the power stablization loop. Finally, a fraction of the transfer beam reflected by the micro-oscillator was sent to an OOL PD, which monitored the transfer beam power noise. Despite having the same laser source for practical reasons, the power fluctuations of the transfer and sensing beams were not correlated after transmission through the optical fibers. The micro-oscillator mirror used in this experiment consisted of a circular mirror pad with a radius of 60 μm, supported by a cantilever with a length of 200 μm, width of 12 μm, and thickness of 220 nm (picture displayed on the bottom part of Fig. 1). The mirror pad comprised 23 alternating layers of GaAs and $Al_{0.92}Ga_{0.08}As$, forming a distributed Bragg reflector with a total thickness of 4.2 μm, a transmission of 250 ppm, and a reflectivity of ≈ 99.97% for a wavelength of 1064 nm. A measurement of the micro-oscillator's optomechanical response resulted in a mass of 190 ng and a fundamental longitudinal resonance frequency of 151 Hz. Information on similar micro-oscillators can be found in [11]. This micro-oscillator was chosen as the movable mirror for this setup due to its low mass and low resonance frequency, which are desirable to increase the mirror displacement caused by the radiation pressure from the transfer beam, and hence increase the signal-to-noise ratio in the in-loop sensor [10]. To suppress the influence of vibrational noise, the complete experimental setup, including the vacuum chamber, was mounted on top of an optical table supported by pneumatic feet, which provided vertical and horizontal isolation for frequencies above 4 Hz. To reduce the vibrational noise coupling to the interferometer even further, the in-vacuum breadboard was mounted on top of three compact isolation feet from the company Newport (model VIB100). They provided vertical isolation above 11 Hz and horizontal isolation above 8.5 Hz. The sensing beam power hitting the micro-oscillator was ≈ 7 mW, which was at least six times smaller than the transfer beam power. Hence, its radiation pressure noise did not limit the sensitivity of this experiment. All measurements were performed with a maximum pressure of 10^{-4} mbar in the vacuum chamber to reduce thermal noise due to viscous damping.

In the first part of the experiment, noise sources and their coupling to the interferometer readout were investigated and minimized. This was an important step since the interferometer

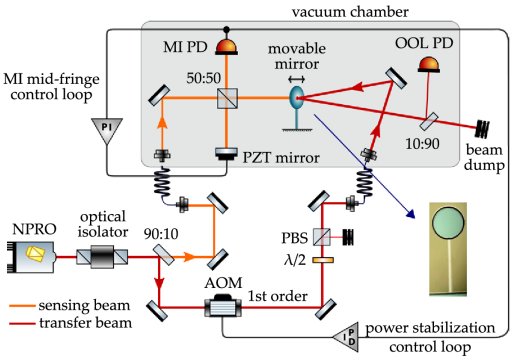

Fig. 1. Schematic of the experimental setup. An NPRO laser was split into the transfer beam (red trace) and sensing beam (orange trace) by a beam splitter. Both beams were guided to a vacuum chamber, where a breadboard containing the movable mirror and the Michelson interferometer was located. The MI PD was the in-loop sensor for two control loops: the Michelson Interferometer (MI) loop, which used a PZT as an actuator, and the power stabilization loop, which used an AOM as an actuator.

displacement noise will be imprinted on the OOL beam (transfer beam) by the power stabilization control loop, and will set a limit to the maximum power stability that can be achieved with this scheme. To avoid the high thermal noise from the micro-oscillator mirror, the technical noise sources were investigated in a configuration where the micro-oscillator was substituted by a rigidly fixed standard high reflective mirror. The blue curve in Fig. 2 shows the interferometer sensitivity after the optimization of several technical noise sources. The main contributions for the displacement noise were residual vibrational noise at frequencies below 100 Hz, and a sum of electronic noise and sensing beam power noise coupling at the mid-fringe operation point for frequencies above 100 Hz. The broad peak around 7 Hz was caused by the vertical and horizontal resonances of the VIB100 isolation feet. The coupling path of this noise was not fully understood, and long-term observations in the displacement noise showed variations of the peak height that were independent of the setup configuration. These observations led to the conclusion that the driving forces of these resonant motions are not long-term stable and are linked to changes in the vibrations of the laboratory building. The displacement noise measured with the micro-oscillator mirror is shown by the red curve, together with its thermal noise fit (black curve). The thermal noise was calculated as a sum of the structural [12] and viscous damping contributions of the micro-oscillator mirror at room temperature. This fit resulted in a structural quality factor for the fundamental longitudinal mode of 6×10^3. The fit shows that the displacement noise measured with the micro-oscillator is thermal noise limited in the frequency range between 15 Hz and a few kHz. This contribution could be reduced by operating the experiment at cryogenic temperatures. However, due to the increase in complexity and non-availability of a cryostat, this experiment was always operated at room temperature. For alignment reasons, the transfer beam was turned on during the measurement displayed by the red curve, with a power of 48 mW. The radiation pressure displacement caused by its power noise in this case was non-negligible, and it was the reason for the excess displacement noise at frequencies below 5 Hz. In conclusion, the measurements show that, apart from

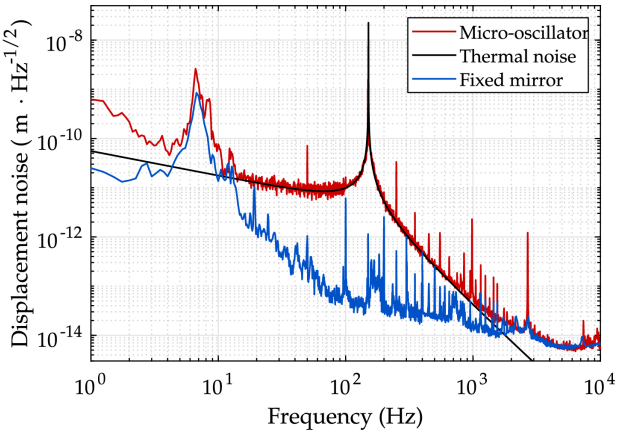

Fig. 2. Amplitude spectral density (ASD) of the interferometer displacement noise measured with the fixed mirror and with the micro-oscillator mirror. The black curve shows the thermal noise fit for the micro-oscillator.

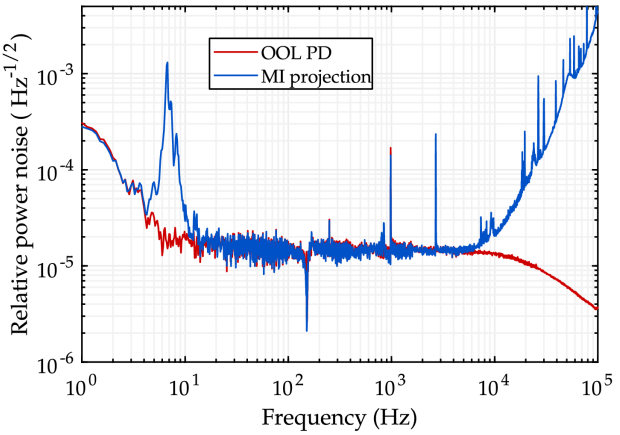

Fig. 3. ASD of the free running RPN of the transfer beam (with white noise injection) measured by the OOL PD (red curve), and the corresponding interferometer displacement projected to the RPN of the out-of-loop beam (blue curve).

the 7 Hz peak, the interferometer was thermal noise limited for frequencies below 1 kHz.

After characterizing the interferometer displacement noise, the second part of the experiment demonstrated that the interferometer can be used as a sensor for power fluctuations of the transfer beam. For this demonstration, the mean power on the transfer beam was set to 48 mW, since it should be far below the damage threshold of the micro-oscillator. Apart from frequencies below 5 Hz, the NPRO absolute power fluctuations corresponding to this mean power are too small to drive the oscillator's motion above the interferometer readout noise. For this reason, a broadband white noise was added to the NPRO's RPN by the AOM. Hence, from now on, the term "free running" in this Letter will refer to the effective free running noise of the transfer beam after the addition of white noise. The result of this demonstration is shown in Fig. 3, where the free running RPN of the OOL beam measured with the OOL PD (red curve) is plotted against the interferometer displacement fluctuations projected to the OOL beam (blue curve, in-loop measurement). This projection was performed by converting the voltage of the MI PD to interferometer displacement (at the mid-fringe operation point), and subsequently by converting the obtained displacement to transfer beam power via the optomechanical response of the micro-oscillator. The curves show that, apart from the 7 Hz peak, the in- and out-of-loop power noise measurements overlap for frequencies below 5 kHz. At higher frequencies, the in-loop measurement is still dominated by sensing noise, which is approximately flat in this frequency regime, and therefore the in-loop projection follows a shape of approximately f^2, as expected from the radiation pressure displacement after the fundamental longitudinal resonance frequency.

Finally, in the third part of the experiment, the power stabilization control via radiation pressure sensing was turned on. The OOL performance, measured by the OOL PD, is shown in Fig. 4. The red curve displays the free running RPN, while the orange, green, and blue curves display the power noise when the loop is turned on for different mean powers $\bar{P}_t$ in the transfer beam. In all measurements, a broadband white noise was imprinted to the transfer beam (with an amplitude two times larger than the one described in Fig. 3). The dashed curves accompanying the measurements were calculated as an uncorrelated sum of the expected free running noise reduction by the

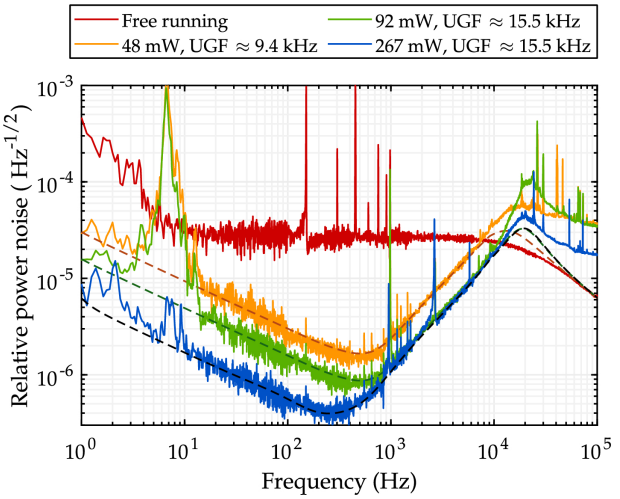

Fig. 4. ASD of the RPN measured by the OOL PD when the power stabilization control loop is turned off (red) and when the loop is on for different transfer beam powers. The dashed curves were calculated as an uncorrelated sum of the micro-oscillator's thermal noise projected to RPN and the expected free running noise reduction by the stabilization control loop.

control loop gain, and the micro-oscillator's thermal noise fit projected to RPN of the OOL beam [10]:

$$\mathrm{RPN}_{\mathrm{ool,tn}} = \frac{c\, f_0}{\bar{P}_t}\sqrt{\frac{2\pi k_B T m}{Q f}}, \tag{1}$$

where f_0 is the longitudinal resonance frequency, m is the mass, Q is the structural quality factor, T is the temperature, k_B is the Boltzmann constant, and c is the speed of light. The stability for frequencies below 500 Hz was limited by the micro-oscillator's thermal noise and, as expected, it had a $f^{-1/2}$ dependence. At higher frequencies, the stability was limited by the loop gain. The results show that in the regime where the stability was thermal noise limited, the RPN was reduced by increasing the transfer beam mean power. This reduction is expected since the absolute power modulation applied by the control loop to the transfer beam to compensate for the micro-oscillator's thermal

noise motion is independent of the transfer beam mean power. It is important to note that the measurements displayed by the orange and green curves were performed by keeping the same electronic gain in the electronic feedback controller, and by increasing the transfer beam power using the attenuation stage located after the AOM (Fig. 1). In this manner, the transfer function from power modulation imprinted by the AOM to absolute power modulation after the attenuation stage increased linearly with power. As a result, the magnitude of the open loop transfer function, and therefore the UGF, was also increased with power. This led to a higher suppression of the free running power noise at frequencies above 500 Hz in the green curve with respect to the orange curve. Since the loop was close to instability for UGFs above 20 kHz, the electronic gain was reduced for measurements with powers above 100 mW such as to keep the UGF at 15.5 kHz, as shown by the blue curve. Note that since the blue and green curves were measured with the same UGF, they overlap in the region where the stability is limited by the loop gain. A discrepancy above the UGF can be observed, where the noise in the blue curve is smaller than in the green one, which is most likely due to its lower electronic gain. At the maximum transfer beam power of 267 mW, an RPN of $3.7 \times 10^{-7}\ \mathrm{Hz}^{-1/2}$ was achieved at 250 Hz, corresponding to a free running noise reduction by a factor of 73. As noted above, the driving force for the 7 Hz resonance of the vibration isolation was unpredictably varying in the laboratory. This is most likely the reason for the reduced 7 Hz peak in the 267 mW measurement since, besides the transfer beam power, all experimental conditions were identical to the other measurements. An interesting remark is that a peak at the fundamental longitudinal resonance frequency of the micro-oscillator is present in the free running noise measurement, as well as its corresponding first five harmonics. Those peaks are suspected to be caused by beam jitter on the OOL photodiode. They are, however, not present in the measurements where the power stabilization loop is turned on because the micro-oscillator's longitudinal motion, and hence the beam jitter, is reduced by the control loop gain. Finally, it is worth noting that the transfer/sensing beam was not completely centered to the micro-oscillator's mirror pad, which can be seen by the coupling of the peaks corresponding to the yaw and pitch motion (952 Hz and 2640 Hz) in the stabilized power noise measurement (coupling via thermal noise motion). For transfer beam powers above 200 mW, power noise measurements and power stabilization of the NPRO's free running noise without the addition of white noise were demonstrated for frequencies up to 2 kHz (results not shown in this Letter). In these measurements, the stability was solely limited by the interferometer displacement noise, since the loop gain was sufficient to suppress the NPRO's noise. A similar thermal noise behavior was observed, and an RPN of $2.5 \times 10^{-7}\ \mathrm{Hz}^{-1/2}$ was achieved at 730 Hz for a power of 267 mW, corresponding to a noise reduction factor of four. In summary, the measurements were well understood, and they agree very well with the projections of the expected RPN for this experiment.

The straightforward path to achieve higher power stability at frequencies where the experiment was thermal noise limited is to further increase the transfer beam power. Here, the maximum power was set by the limit in the pitch degree of freedom adjustment capability in the micro-oscillator mirror mount. This pitch range is important to compensate for the oscillator's mirror pad static pitch displacement introduced by the radiation pressure exerted by the mean transfer beam power, and to keep the mirror surface normal to the incident beams. This displacement was calculated to be $\approx 11\ \mu\mathrm{m}$ for 285 mW, which corresponds to a pitch angle of 3.2° with respect to its relaxed position. Experiments with similar mirrors have set a lower limit of 500 mW for their power damage threshold. In future experiments, however, the damage threshold and breaking mechanism should be investigated since this is an important step towards an optimal design for a movable mirror that can stand high power.

In conclusion, the successful implementation of the radiation pressure scheme for laser power stabilization shown in this Letter paves a way for achieving high power stability in future experiments. An important step towards this goal is to design a movable mirror optimized for the purpose of power stabilization of high laser power (a couple of Watts or even hundreds of Watts). The power tolerance of the mirror is a crucial aspect to be considered, since the achievable power stability is directly proportional to the transfer beam power. Another relevant aspect is to reduce the thermal noise contribution of the mirror. This could be achieved in a cryogenic environment and by increasing the structural quality factor of the mirror, or by increasing the mirror susceptibility, since the achievable power stability is proportional to the square root of its magnitude [10]. In addition to that, alternative mirror designs should also be investigated. A mirror with a displacement constrained only to the longitudinal motion would dispense the need for a realignment in the pitch degree of freedom. An optimal mirror implemented in this experiment with a cold environment could result in an RPN on the order of $10^{-10}\ \mathrm{Hz}^{-1/2}$ at low frequencies [10], which will be essential for future gravitational wave detectors. Finally, such a mirror could also lead to the experimental observation of a strong bright squeezed beam.

Funding. FP7 People: Marie-Curie Actions (606176); National Science Foundation (PHY-1806634); Deutsche Forschungsgemeinschaft (EXC-2123 Quantum Frontiers 390837967).

Disclosures. The authors declare no conflicts of interest.

REFERENCES

1. Y. Wang, M. Nikodem, E. Zhang, F. Cikach, J. Barnes, S. Comhair, R. A. Dweik, C. Kao, and G. Wysocki, Sci. Rep. **5**, 9096 (2015).
2. Q.-X. Li, S.-H. Yan, E. Wang, X. Zhang, and H. Zhang, AIP Adv. **8**, 095221 (2018).
3. N. Matsumoto, "Classical pendulum feels quantum back-action," Ph.D. thesis (University of Tokyo, 2016).
4. G. M. Harry, and The LIGO Scientific Collaboration, Class. Quantum Gravity **27**, 084006 (2010).
5. P. Kwee, B. Willke, and K. Danzmann, Opt. Lett.**34**, 2912 (2009).
6. H. Vahlbruch, D. Wilken, M. Mehmet, and B. Willke, Phys. Rev. Lett.**121**, 173601 (2018).
7. P. Kwee, B. Willke, and K. Danzmann, Opt. Lett.**33**, 1509 (2008).
8. Y. Yamamoto, N. Imoto, and S. Machida, Phys. Rev. A**33**, 3243 (1986).
9. A. Khalaidovski, A. Thüring, H. Rehbein, N. Lastzka, B. Willke, K. Danzmann, and R. Schnabel, Phys. Rev. A**80**, 053801 (2009).
10. M. T. Nery, S. L. Danilishin, J. R. Venneberg, and B. Willke, Opt. Lett.**45**, 3969 (2020).
11. R. Singh, G. D. Cole, J. Cripe, and T. Corbitt, Phys. Rev. Lett.**117**, 213604 (2016).
12. P. R. Saulson, Phys. Rev. D**42**, 2437 (1990).